 doi:10.20944/preprints201710.0077.v1

Article

Global Calibration of Multi-Cameras Based on Refractive Projection and Ray Tracing

Mingchi Feng [1,*], Xiang Jia [1], Jingshu Wang [2], Song Feng [1] and Taixiong Zheng [1]

[1] School of Advanced Manufacturing Engineering, Chongqing University of Posts and Telecommunications, Chongqing 400065, China; jx_199209@163.com (X.J.); fengsong@cqupt.edu.cn (S.F.); zhengtx@cqupt.edu.cn (T.Z.)

[2] College of Mechanical Engineering, Chongqing University of Technology, Chongqing 400054, China; donot@cqut.edu.cn

* Correspondence: fengmc@cqupt.edu.cn; Tel.: +86-185-8138-1350

Abstract: Multi-cameras system is widely applied in 3D computer vision especially when multiple cameras are distributed on both sides of the measured object. The calibration methods of multi-cameras system are critical to the accuracy of vision measurement and the key is to find an appropriate calibration target. In this paper, a high-precision camera calibration method for multi-cameras system based on transparent glass checkerboard and ray tracing is described, which is used to calibrate multiple cameras distributed on both sides of the glass checkerboard. Firstly, the intrinsic parameters of each camera is obtained by Zhang's calibration method. Then, multiple cameras capture several images from the front and back of the glass checkerboard with different orientations, and all images contain distinct grid corners. As the cameras on one side are not affected by the refraction of glass checkerboard, extrinsic parameters can be directly calculated. However, the cameras on another side are influenced by the refraction of glass checkerboard, and the direct use of projection model will produce calibration error. A multi-cameras calibration method using refractive projection model and ray tracing is developed to eliminate this error. Furthermore, both synthetic and real data are employed to validate the proposed approach. The experimental results of refractive calibration show that the error of the 3D reconstruction is smaller than 0.2 mm, the relative errors of both rotation and translation are less than 0.014%, and the mean and standard deviation of reprojection error of 4-cameras system are 0.00007 and 0.4543 pixel. The proposed method is flexible, high accurate, and simple to carry out.

Keywords: camera calibration; multi-cameras system; ray tracing; glass checkerboard; bundle adjustment

1. Introduction

Multi-cameras system (MCS) have many merits over single camera because they can cover a wider and overall field of view (FOV), which makes MCS increasingly prevalent in industrial vision measurement [1,2], visual navigation [3,4], security monitoring [5], etc. With the advantages of flexibility, cost performance and high precision, industrial vision measurement using MCS has been widely studied in many applications, such as car body-in-white inspections [6], deformation and displacement measurement [7,8]. The measurement of dimension, shape, and deformation is a dynamic process, so all cameras should observe the part surface from different viewpoints simultaneously (one-shot image acquisition) and dynamically reconstruct the 3D shape of the whole object. This kind of MCS includes multiple cameras sharing an overlapping FOV at different orientations. In the special case, these cameras are distributed in the opposite direction. Accurate calibration of multi-cameras is quite significant [9], since the calibration results determine the mapping relationship between world points and their image projections. Generally speaking, the overall performance of the MCS strongly depends on the accuracy of the camera calibration.

The calibration methods of MCS are divided into two categories: metric calibration and self-calibration. The proposed method, using knowledge of the scene such as calibration pattern to calculate stable and accurate calibration results, belongs to the metric approaches rather than self-calibration. Several patterns were proposed for multi-cameras metric calibration, which can be grouped into three main categories: 3D calibration target, planar target, and one-dimensional target.

A representative calibration scenario of multi-cameras begins by placing calibration target in the overlapping FOV of the cameras to provide a projection relationship between image and world points [10]. The standard calibration target is a planar pattern, such as checkerboard. Zhang [11] proposed a flexible new technique to easily calibrate single camera using a planar pattern, which had been used in other multi-cameras calibration [12-15]. Dong [12] presented an extrinsic calibration method for a non-overlapping camera network based on close range photogrammetry. This method calibrated the extrinsic parameter of multi-cameras using a vast number of encoded targets pasted on the wall. Baker [13] used textures printed on either side of a board to calibrate dozens of cameras. One side of the board was printed by a set of lines, while the other side of the board was printed by a set of boxes with one missing in the middle. Belden [14] described refractive calibration procedure applied to calibrate MCS for fluid experiments. This method contributed to volumetric multi-camera fluid experiments, where it was desirable to avoid tedious alignment of calibration grids in multiple locations and a premium was placed on accurately locating world points. In reference [15], a MCS had been developed to measure the shape variations and the 3D displacement field of a sheet metal part during a Single Point Incremental Forming operation. The calibration of the multi-cameras determining camera parameters were described in their paper using planar calibration target. The planar calibration pattern limits the distribution of multiple cameras, especially, when multiple cameras distributed on both sides of planar pattern. The uneven printed pattern can also affect the accuracy of camera calibration.

In addition, 1D calibration target and 3D calibration target are also widely used in the calibration of MCS, such as Figures 1 and 2. 1D target-based camera calibration was firstly proposed by Zhang [16]. Compared with conventional 2D or 3D target-based camera calibration, the main advantage of 1D target-based camera calibration is that it doesn't need to know the 2D or 3D coordinates of markers, which significantly simplifies the manufacturing process of calibration targets. More importantly, without self-occlusion problem, the 1D calibration target can be observed by all cameras in the MCS. The advantage is that all cameras are calibrated simultaneously, which avoids the accumulation of errors when multi-cameras calibration is performed in steps or groups. Therefore, this camera calibration method has been widely used by many MCS [10,17-21]. However, the disadvantages of 1D calibration target including [21]: 1) In the construction of the 1D pattern, it is not possible to guarantee the exact linearity of the points, hurting one of the main assumptions of the adopted model. 2) Another source of error is the tool used to extract the points of the calibration pattern, which cannot achieve the same accuracy of corner extraction in 2D target-based camera calibration.

A typical 3D calibration target is composed of multiple 1D patterns. Shen [10] presented a complete calibration methodology using a novel nonplanar target for rapid calibration of inward-looking visual sensor networks. The calibration target consists of a large central sphere with smaller spheres of different colors mounted on support rods. A flexible method constructing a global calibration target with circular targets was proposed by Gong [2]. Shin [22] described a multi-cameras calibration method using a 3-Axis frame and wand. In this study, the calibration parameters were estimated using the direct linear transform (DLT) method from the three-axis calibration frame. However, the main source of error in this kind of 3D calibration target is attributed to errors of ellipse fitting caused by image noise and lighting conditions. The accuracy of center extraction cannot achieve the same accuracy of corner extraction in planar pattern [21]. This type of 3D calibration target has the same disadvantage as the 1D calibration target. Another kind of 3D calibration target consists of multiple planar pattern, such as the works of Long [23] and Xu [24]. Unfortunately, in MCS like Figure 2, it is hard to use this calibration target, which can't be viewed by all the cameras

Preprints (www.preprints.org) | NOT PEER-REVIEWED | Posted: 12 October 2017 doi:10.20944/preprints201710.0077.v1

simultaneously. This 3D calibration target limits the distribution of multiple cameras, which restricts its application.

In order to overcome the shortcomings of the foregoing methods, and guarantee high-accuracy and convenience of the multi-cameras calibration, we propose a novel method of global calibration for multiple cameras with overlapping FOVs. This method adopts a planar calibration target made of transparent glass, and the checkerboard pattern is printed on one side of the glass panel. Multiple cameras are distributed on both sides of the calibration target and towards the calibration target (Figure 5). This kind of configuration is useful to get one-shot 3D shape of the whole object. The cameras in front of the calibration target are not affected by the refraction, and the traditional Zhang's method can be used to calibrate the intrinsic and extrinsic camera parameters. But, the cameras in the rear of the calibration target are influenced by refraction, and the direct use of Zhang's method will cause calibration error. The refraction of glass will affect the accuracy of multi-cameras calibration results. This proposed method uses refractive projection model and ray tracking to eliminate the error of refraction. Based on the 3D position accuracy of the corner point on the glass checkerboard being as high as 0.0015mm, the proposed multi-cameras calibration in this paper can achieve high-accuracy and flexibility.

The remainder of this paper is organized as follows: Section 2 introduces the basic mathematical model of MCS and ray tracking. In Section 3, the proposed calibration method of multi-cameras based on refractive projection model and ray tracing is described. Section 4 presents a series of experiments (synthetic and real data) to verify the feasibility and accuracy of the proposed approach. Single-camera experiment verifies feasibility of the refractive projection model and calibration of extrinsic camera parameters. Two-camera experiment confirms the accuracy of calibration of extrinsic camera parameters and refractive index. Four-camera experiment verifies the performance of our method used in the actual MCS. The conclusions are indicated in Section 5.

2. Mathematical Model of Camera and Ray Tracking

This section briefly introduces the basic concepts used in the calibration of single camera and MCS. Then, the refractive projection model and ray tracking used in this paper will be described.

2.1. Camera Model

An ideal camera is modeled by the pinhole imaging. The relationship between a 3D point in world coordinate and the same point in camera coordinate is approximated by means of the rotation matrix and transformation matrix, as shown in Equation (1).

$$\begin{bmatrix} X_C \\ Y_C \\ Z_C \end{bmatrix} = R*P+T = R*\begin{bmatrix} X \\ Y \\ Z \end{bmatrix} + T \tag{1}$$

The projection of the point in camera coordinate on the image is $p = [u, v]^T$, which obeys Equation (2).

$$\lambda \begin{bmatrix} u \\ v \\ 1 \end{bmatrix} = K \begin{bmatrix} X_C \\ Y_C \\ Z_C \end{bmatrix} \text{ with } K = \begin{bmatrix} f_u & \gamma & u_0 \\ 0 & f_v & v_0 \\ 0 & 0 & 1 \end{bmatrix} \tag{2}$$

where, $P = [X, Y, Z]^T$ are the world coordinates of a 3D point and $[X_C, Y_C, Z_C]^T$ are its camera coordinates, and $[u, v]^T$ are its pixel image coordinates. λ denotes a nonzero scale factor. $[u_0, v_0]^T$ denote the principal point in the imaging plane with the unit of pixel. K is the matrix of intrinsic parameter. f_u and f_v represent the focal length in pixels along the image axes u and v, while γ is the skew coefficient defining the angle between the u and v pixel axes. R and T, called the extrinsic parameters, are the rotation matrix and the translation vector from world coordinate frame

Preprints (www.preprints.org) | NOT PEER-REVIEWED | Posted: 12 October 2017 doi:10.20944/preprints201710.0077.v1

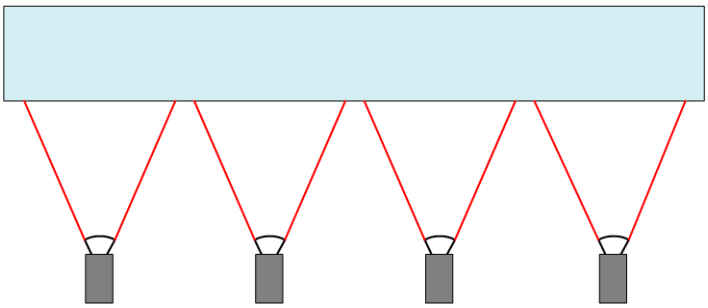

Figure 1. Multi-cameras system without overlapping FOV.

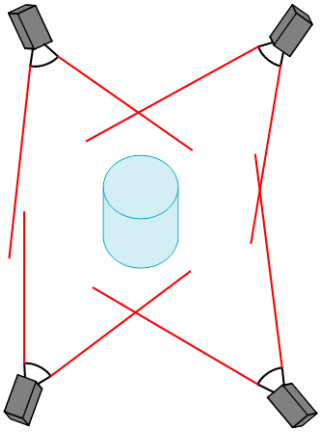

Figure 2. Multi-cameras system with overlapping FOV.

to camera coordinate frame, respectively.

However, the real camera projection is not ideal, particularly when a commercial lens is used. Therefore, the lens distortion on the imaging has to been taken into account. Commonly, only first-order or second-order distortion model is adopted to correct the radial distortion [11,25,26]. More rigorously, the radial distortion and tangential distortion should be adopted to correct the lens distortion [9,27]. After considering the lens distortion, the new normalized point coordinates $[x_d, y_d]^T$ are defined as follows.

The distortion-free and the distorted normalized image coordinates are $[x, y]^T$ and $[x_d, y_d]^T$, respectively.

$$\begin{bmatrix} x \\ y \end{bmatrix} = \begin{bmatrix} X_c / Z_c \\ Y_c / Z_c \end{bmatrix} \tag{3}$$

$$\begin{bmatrix} x_d \\ y_d \end{bmatrix} = (1 + k_1 r^2 + k_2 r^4 + k_5 r^6) x_n + dx \tag{4}$$

$$dx = \begin{bmatrix} 2k_3 xy + k_4 (r^2 + 2x^2) \\ k_3 (r^2 + 2y^2) + 2k_4 xy \end{bmatrix} \quad \text{with} \quad r^2 = x^2 + y^2 \tag{5}$$

where, $1 + k_1 r^2 + k_2 r^4 + k_5 r^6$ is radial distortion and dx is the tangential distortion. k_1, k_2, k_5 are the coefficients of radial distortion, and k_3, k_4 are the coefficients of tangential distortion. We will use $\mathrm{D} = [k_1, k_2, k_3, k_4, k_5]$ to represent the vector of distortion coefficients in this paper.

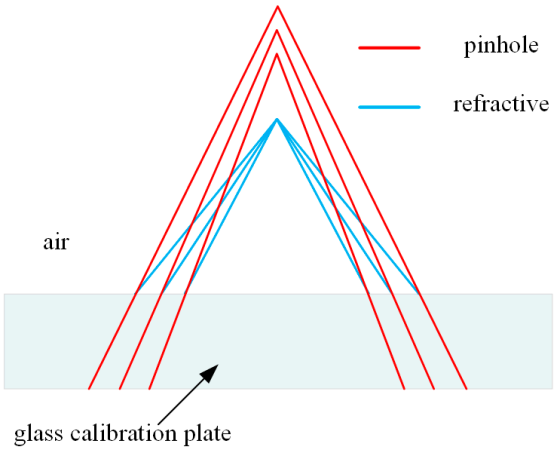

Figure 3. Schematic of imaging through glass using pinhole and refractive projection model.

Preprints (www.preprints.org) | NOT PEER-REVIEWED | Posted: 12 October 2017 doi:10.20944/preprints201710.0077.v1

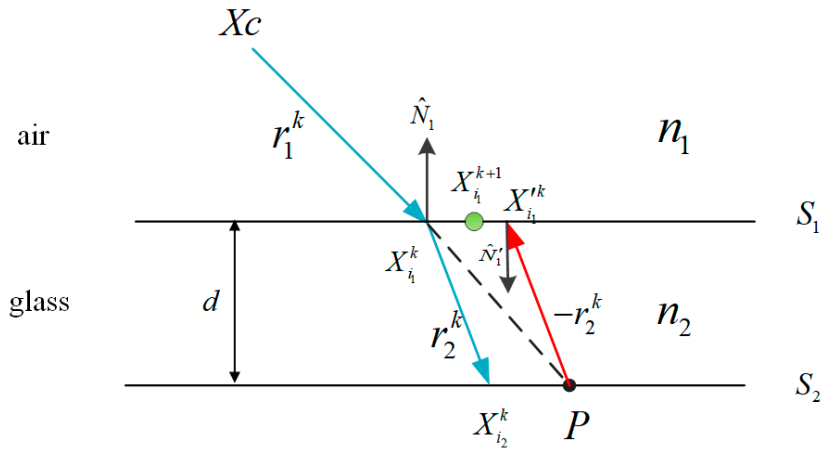

Figure 4. Schematic of ray tracking method

Based on the descriptions above, a 3D point P in the world coordinate system (WCS)can be projected to a 2D point p in the image coordinate system using the following projection equation:

$$p = f(K, R, T, D, P) \tag{6}$$

2.2. Refractive Projection and Ray Tracking

Usually, the aforementioned pinhole model can meet the requirements of the camera calibration, but the transparent glass checkerboard is applied in our method. The direct application of the pinhole model between world and image points is erroneous as the refraction of light must be considered in our MCS. As shown in Figure 3, if the rays emanating from the world points are drawn along the path taken in the glass (red line), they do not meet in a single point in the air. In this case, the accurate pinhole model will also lead to error that is exacerbated for cameras when image planes are not parallel to the glass checkerboard. In Belden's work [14], the image plane is angled relative to the interface, which results in relatively high calibration error when the pinhole model is applied. The reprojection error using pinhole model in the experiment of our paper is also the same order of magnitude. The non-ignorable error keeps us from adopting the pinhole model for multi-cameras calibration using glass checkerboard.

In order to eliminate the calibration error caused by refraction, the refraction in the optical paths must be appropriately considered for when projecting 3D points into cameras through glass. We need to find the intersection of each ray with the refractive interface between glass and air, and project the intersection points to pinhole camera. In this paper, we adopt the ray tracking method proposed by Muslow that initializes the intersection points using an alternating forward ray tracing (AFRT) method [28]. To calculate the intersection of rays with glass surfaces, the points that simultaneously satisfy the equation of a line and the plane equation defining the surface geometry of glass should be solved. A point on a line along the direction of a given ray $\hat{\mathbf{r}}$ is defined in the Equation (7).

$$X(t) = X_0 + t\hat{\mathbf{r}} \tag{7}$$

The refractive index of air and glass is n_1 and n_2 $(n_2 > n_1)$. Assume that the refractive index of air is equal to one, and the relative refractive index of glass $(n = \frac{n_2}{n_1} = n_2)$ is one of the optimized parameters. The thickness of glass is d. $\hat{\mathbf{r}}_\mathbf{i}$ and $\hat{\mathbf{N}}$ denote the direction of the incident ray and the normal vector of refractive surface, respectively. The direction of the refracted ray $\hat{\mathbf{r}}_\mathbf{t}$ is given by:

$$\hat{\mathbf{r}}_\mathbf{t} = n\hat{\mathbf{r}}_\mathbf{i} + \left[n\hat{\mathbf{N}} \cdot \hat{\mathbf{r}}_\mathbf{i} - \sqrt{1 - n^2\left[1 - (-\hat{\mathbf{N}} \cdot \hat{\mathbf{r}}_\mathbf{i})^2\right]} \right] \hat{\mathbf{N}} \tag{8}$$

Figure 4 depicts the algorithm of ray tracing in order to find the intersection of rays with planar glass surface. The procedure of ray tracing is described as follows:

Preprints (www.preprints.org) | NOT PEER-REVIEWED | Posted: 12 October 2017 doi:10.20944/preprints201710.0077.v1

1. The procedure is initialized by k = 1. r_1^k denotes the direction of the line connecting the camera center X_C and the 3D point P. We could find the intersection of r_1^k and S_1 at the point $X_{i_1}^k$.
2. When n_1 and n_2 have been known, we could find the r_2^k using the Equation (8), which intersects S_2 at the point $X_{i_2}^k$.
3. The ray $-r_2^k$ is projected from P to interface S_1, and parallel to r_2^k but opposite in direction.
4. Finally, the ray $-r_2$ is intersected with S_1, resulting the point $X_{i_1}'^k$.
5. If the distance $\Delta X_{i_1}^k = \left|X_{i_1}^k - X_{i_1}'^k\right|$ between the $X_{i_1}^k$ and $X_{i_1}'^k$ is larger than the tolerance, the above procedures would be reiterated, and the point at $\frac{1}{2}\left(X_{i_1}^k + X_{i_1}'^k\right)$ is defined as $X_{i_1}^{k+1}$. Otherwise, the optimal solution of the intersection of r_1^k and S_1 is found.

In addition to the intrinsic and extrinsic parameters of the camera, the main parameters affecting the projective ray include the refractive index and thickness of refraction glass. The thickness of the glass can be accurately measured, while refractive index of different glass is slightly different, and most glass refractive index is unknown. Through the above discussion, the Equation (6) can be converted to the Equation (9) with refraction.

$$p_r = f_r(K, D, R, T, P, n) \tag{9}$$

where, p_r and f_r represent the image points generated by the refraction and the refractive projection model, respectively.

3. The Proposed Calibration Method

3.1. Multi-camera Calibration Based on Refractive Projection

In the previous section, we introduced the camera model and the refractive projection, which are combined to calibrate the MCS in this section. In our work, the single camera model is extended to the modeling and calibration of a MCS made up of more than two cameras. Without loss of generality, the MCS will be explained by the particular case of a 4-cameras system, which is also used in the calibration experiments described in the present paper. The MCS is shown in Figure 5, and the object in the center is the glass calibration plate. One side of the glass is printed with a checkerboard pattern, which can be seen from both sides of the calibration plate. Four cameras are distributed on both sides of the calibration plate. These cameras are grouped into two pairs, pair I including cameras 1 and 2, and pair II including cameras 3 and 4. The cameras of pair I directly project the 3D point on calibration plate to image without refraction (Equation 6), while the cameras of pair II for imaging through the reflection of glass (Equation 9), which can lead to calibration errors. The errors can be eliminated by the above refractive projection model and the ray tracing method. Because each camera need to calculate the initial estimation of extrinsic parameters respectively, the major WCS (red) fixed on the upper left corner of the pattern of non-refractive side, and the auxiliary WCS (blue) fixed on the other side of the pattern with refraction. R' and T' denote the rotation and translation between the two WCS.

For a MCS, during the calibration procedure, m $(i = 1,2,\ldots,m)$ images of the calibration plate are taken from each camera at different orientations. For each image, n $(j = 1,2,\ldots,n)$ object points are recognized by the program. In this system, l $(k = 1,2,\ldots,l)$ represents the number of cameras. K_k and D_k respectively represent the intrinsic camera parameters and distortion coefficients of the kth camera. R_{ki} and T_{ki} denote the rotation matrix and translation vector of the ith position of calibration plate relative to the kth camera. p^{kij} is the projection of the jth 3D point on the ith image of the kth camera without refraction. p_r^{kij} denotes the projection of the jth 3D point on the ith image of the kth camera with refraction. The imaging functions are shown as follow.

$$p^{kij} = f(K_k, D_k, R_{ki}, T_{ki}, P_j) \tag{10}$$

Preprints (www.preprints.org) | NOT PEER-REVIEWED | Posted: 12 October 2017 doi:10.20944/preprints201710.0077.v1

$$p_r^{kij} = f_r(K_k, D_k, R_{ki}, T_{ki}, P_j, n) \tag{11}$$

The cameras distributed on both sides of calibration plate use two projection model to solve their extrinsic camera parameters, which are relative to the major WCS or auxiliary WCS. The rotation and translation of each camera need to be aligned to the major WCS. Camera 1 is set as the master camera. The rotation and translation of each camera relative to the master camera is obtained as follows:

$$\begin{cases} R^{1k} = R_{ki} * R_{1i} \\ T^{1k} = T_{ki} - R^{1k} * T_{1i} \end{cases} \text{(without refraction)} \tag{12}$$

$$\begin{cases} R^{1k} = R_{ki} * (R_{1i} * R')^{-1} \\ T^{1k} = T_{ki} - R^{1k} * (R_{1i} * T' + T_{1i}) \end{cases} \text{(with refraction)} \tag{13}$$

R_{1i}, T_{1i} are the extrinsic parameters of the master camera and R^{1k}, T^{1k} are the relative extrinsic parameters of other cameras relative to the master camera.

3.2. Solving Intrinsic Camera Parameters and Initial Estimation of Extrinsic Camera Parameters

The intrinsic parameters of MCS are obtained by Zhang's method. Because the positioning accuracy of the 3D point of calibration target is as high as 0.0015mm, the calibration results are relatively accurate. Before the extrinsic parameters of the system are optimized, it requires an initial estimation of extrinsic camera parameters, which can be obtained using the DLT method described by Hartley [29] or the theory of multi-layer flat refractive geometry presented by Agrawal [30]. The DLT method can only be used when the thickness of glass is relatively small, otherwise the initial estimation of extrinsic parameters will deviate significantly from the truth. The initial estimation of extrinsic parameters gives no considerations to lens distortion and glass refraction, so nonlinear refinement must be applied to the initial estimation aiming at improving accuracy. The best estimate of the camera parameters can be obtained by nonlinear refinement based on the maximum likelihood criterion, such as the Levenberg-Marquardt algorithm. The maximum likelihood estimate for our proposed method can be written as the Equation (14).

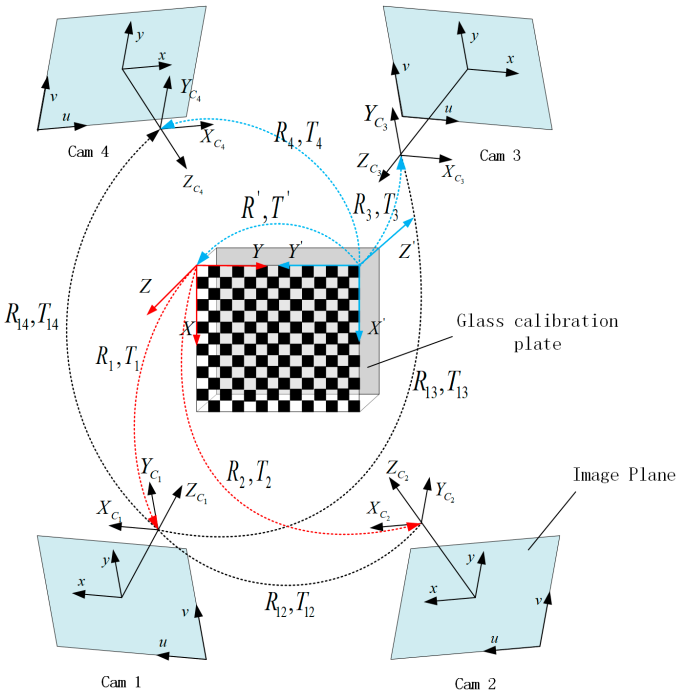

Figure 5. The rotation and translation of 4-cameras system

Preprints (www.preprints.org) | NOT PEER-REVIEWED | Posted: 12 October 2017 doi:10.20944/preprints201710.0077.v1

$$\min_{R_{1i},T_{1i},R^{1k},T^{1k},n}\sum_{k}^{l}\sum_{i}^{m}\sum_{j}^{n}\left((1-w)\left\|x^{kij}-p^{kij}\right\|^2+w\left\|x_r^{kij}-p_r^{kij}\right\|^2\right) \tag{14}$$

Equation (14) shows minimizing of the sum of the reprojection error, which is 2D Euclidean distance between the projected points based on Equations (10) (11) and the actual image points. x^{kij}, p^{kij} are the measured image point and the predicted image point without refraction, and, x_r^{kij}, p_r^{kij} are the measured image point and the predicted image point with refraction. w is the refraction flag. The value 0 of w indicates the projection without refraction, while 1 means the projection with refraction.

A 3D point and corresponding image point can provide two independent equations. Assuming a l-camera system is applied, each camera takes m image of calibration target, and the calibration object contains j known 3D points. The parameters of the equation (14) that need to be solved include $6*m$ rotation and translation parameters of the master camera, $6*(l-1)$ rotation and translation parameters of each camera relative to the master camera, and the refractive index of the glass calibration target. Therefore, $6*(m+l-1)+1$ parameters are solved by $2lmn$ equations, which leads to an over determined system. Taking 4-cameras system as an example, the calibration target contains 182 known 3D points, and each camera captures 20 images. A total of 29120 equations are solved for 139 variables. Assume that the image points are corrupted by independent and identically distributed noise, and the maximum likelihood solution of these variables is obtained.

The nonlinear optimization algorithms commonly employed in bundle adjustment routines require evaluation of the Jacobian matrix of the projection function, defined in Equation (10) and (11). Individual camera is independent of other cameras and calibration points. Therefore, the Jacobian matrix tends to be a very sparse matrix. The sparse structure can be exploited in the minimization routine to improve computational performance.

The quality of the camera calibration is evaluated by computing the mean and the standard deviation of the individual reprojection errors, which is the residual that exists after minimizing Equation (14). Assuming that the individual reprojection error is d and N is the number of equations, the evaluation parameter can be set as follows.

$$\bar{d}=\frac{1}{N}\sum_{k}^{N}d_k \tag{15}$$

$$\sigma_d=\sqrt{\frac{1}{N}\sum_{k}^{N}(d_k-\bar{d})^2} \tag{16}$$

3.3. Summary

The proposed method combines conventional Zhang's method and refractive projection model to realize the calibration of MCS. The global calibration process works as follows:

1. Multiple cameras are installed and their FOV covers the same area of calibration target simultaneously. Intrinsic camera parameters and distortion coefficients of each camera are calibrated independently.
2. In the overlapping FOV of MCS, multiple cameras acquire the image of the calibration target from different orientations. Images captured by each camera contain the front or back of the calibration target.
3. Using the DLT method or the theory of multi-layer flat refractive geometry to obtain the extrinsic camera parameters of each camera relative to their WCS, the extrinsic camera parameters of each camera are unified to the master WCS. The rotation and translation of each camera relative to the master camera is obtained as Equation (12) and (13).
4. The extrinsic camera parameters of the system and the refractive index of the glass are optimized by the bundle adjustment method and the refractive projection model.

Preprints (www.preprints.org) | NOT PEER-REVIEWED | Posted: 12 October 2017 doi:10.20944/preprints201710.0077.v1

4. Experiments and Discussion

The accuracy and robustness of the algorithm discussed in this paper are analyzed using both synthetic and real data. Multiple cameras are usually distributed on both sides of the glass checkerboard and towards the calibration target, so both the direct projection model and refractive projection model are adopted in the proposed calibration method. Since the direct projection model has been verified and applied by many scholars, this article will not discuss it. The experiments mainly analyze the refractive projection model, and the two models are simultaneously applied in the calibration of MCS. In practice, one camera or multiple cameras (such as two cameras) may be deployed on one side of the measured object. In the experiments of synthetic data and real data, we analyze the accuracy of the refractive projection model, which is applied to acquire the refractive index and the extrinsic parameters of single camera and multiple cameras. The extrinsic parameters of each camera are estimated by the DLT method from images of the planar pattern.

4.1 Synthetic Data

The intrinsic parameters and extrinsic parameters of the camera are obtained through the 3D points of the calibration target and corresponding image points. The image points are obtained by the corner detection algorithm in the real data experiment, but the experiment of synthetic data does not need to verify corner detection algorithm. We directly generate the intrinsic and extrinsic parameters of the camera and space points, and obtain the ideal image points using direct projection model (Equation 10) and refractive projection model (Equation 11). The actual image points have the error of corner detection, and the error is simulated by random error of normal distribution. The random error is added to the ideal image point to simulate the real image point.

The simulated camera's image size is 2592x2048 pixels with the principal point at (1296.5, 1024.5) pixels. The focal length along the u and v direction is $f_u = 2604$ pixels and $f_v = 2604$ pixels, respectively. All the distortion coefficients are zero. The skew factor is set to zero. The calibration target is a glass checkerboard with 182 corners (14×13) uniformly distributed and the point interval is 12 mm. The glass checkerboard has a thickness of 4 mm and the refractive index of glass is 1.5. In the generation of the synthetic data, all the images are captured randomly in the range constrained by the distance between object and camera being 300-400 mm and the angles between camera coordinate and world coordinate being $\alpha = (180 \pm 15)^{\circ}$, $\beta = (90 \pm 15)^{\circ}$, $\gamma = (0 \pm 15)^{\circ}$. The world coordinate frame is set on the checkerboard. The basic parameters of the synthetic experiment are basically consistent with the real experiment.

In order to evaluate the robustness of our method with respect to noise, some simulations have been performed, in which noise is added to the ideal image points ranging from 0 to 0.4 pixels. For each noise level, we perform 100 independent trials and each trial contains 20 images. The estimated camera parameters using simulative image points are compared with the ground truth. In this section, the mean relative error of rotation and translation vector is used to assess the calibration accuracy.

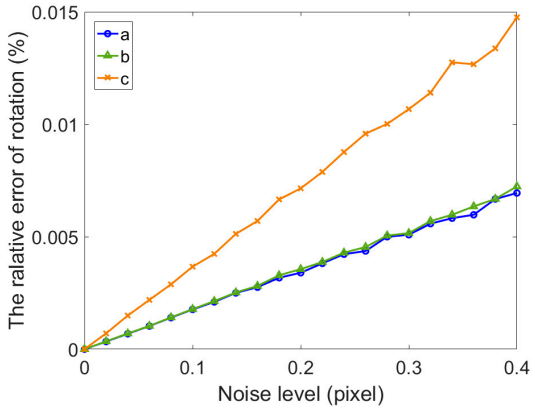

(a)

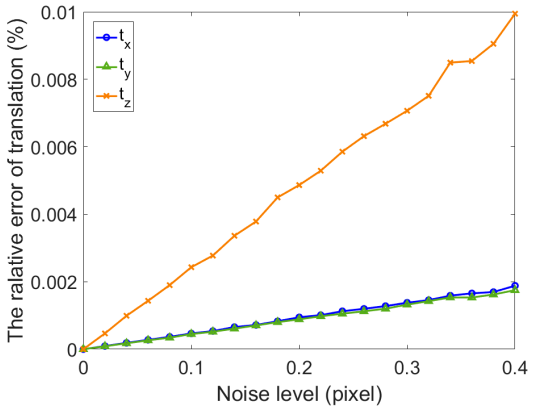

(b)

Preprints (www.preprints.org) | NOT PEER-REVIEWED | Posted: 12 October 2017 doi:10.20944/preprints201710.0077.v1

Figure 6. The relative error of extrinsic parameters for one camera without refraction estimation. (a) Relative error for rotation vector; (b) Relative error for translation vector

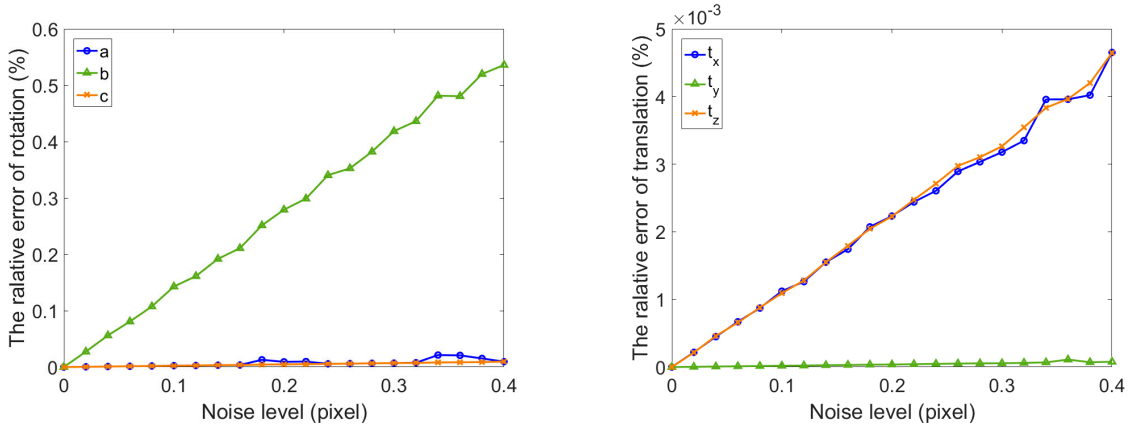

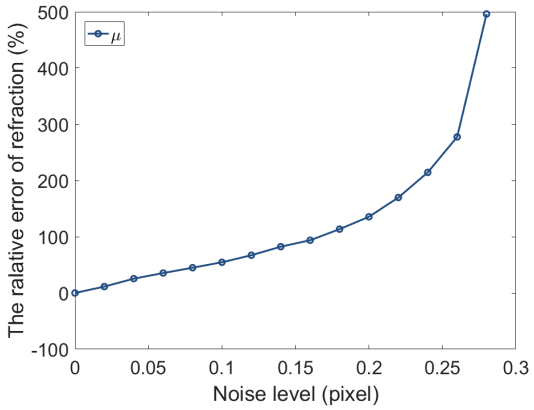

Figure 7. The relative error of extrinsic parameters for one camera with refraction estimation. (a) Relative error for rotation vector; (b) Relative error for translation vector; (c) Relative error for refraction index.

If the rotation vector is $v = \text{Rodrigues}(R)$, the relative errors of rotation and translation vector are $|\nabla v|/\|v\|$ and $|\nabla T|/\|T\|$.

In practice, the thickness of the glass plate is known, while the refractive index is unknown, approximately being equal to 1.5. The smaller change of refractive index has less influence on the image projection, and the refractive effect on the calibration result is relative small compared to the noise. The extrinsic parameters of the single camera are estimated to be divided into two scenarios: with refractive index estimation and without refractive index estimation.

As shown in Figures 6 and 7, whether the refractive index is estimated, the errors of rotation and translation vector for single camera gradually increase with the noise level. The relative error of rotation vector is less than 1.5×10^{-6} and translation error is less than 1×10^{-6} when the refraction index is not estimated ($\mu = 1.5$). The error of extrinsic parameters using fixed refractive index is more consistent and stable than the error using estimated refractive index. It can be saw from the Figure 7a, b that the calibration results in all directions are inconsistent. The growth rate of the error in y direction is inconsistent with the x and z direction. The results are shown in Figure 7c, the error of refractive index increases dramatically, which can be considered incorrect. There is reason to believe that this result is due to an incorrect estimation of refractive index. When the thickness of glass is small, a single camera cannot accurately estimate the refractive index. The main cause of this problem is that the ray direction is less restrictive. If the cameras can be added in different orientations, the estimated accuracy of refractive index can be improved. Meanwhile, we can also find in Figures 6 and 7 that the extrinsic parameters of the camera are accurate in both cases. When the extrinsic parameters of single camera are estimated, the fixed refractive index can obtain higher accuracy.

Preprints (www.preprints.org) | NOT PEER-REVIEWED | Posted: 12 October 2017 doi:10.20944/preprints201710.0077.v1

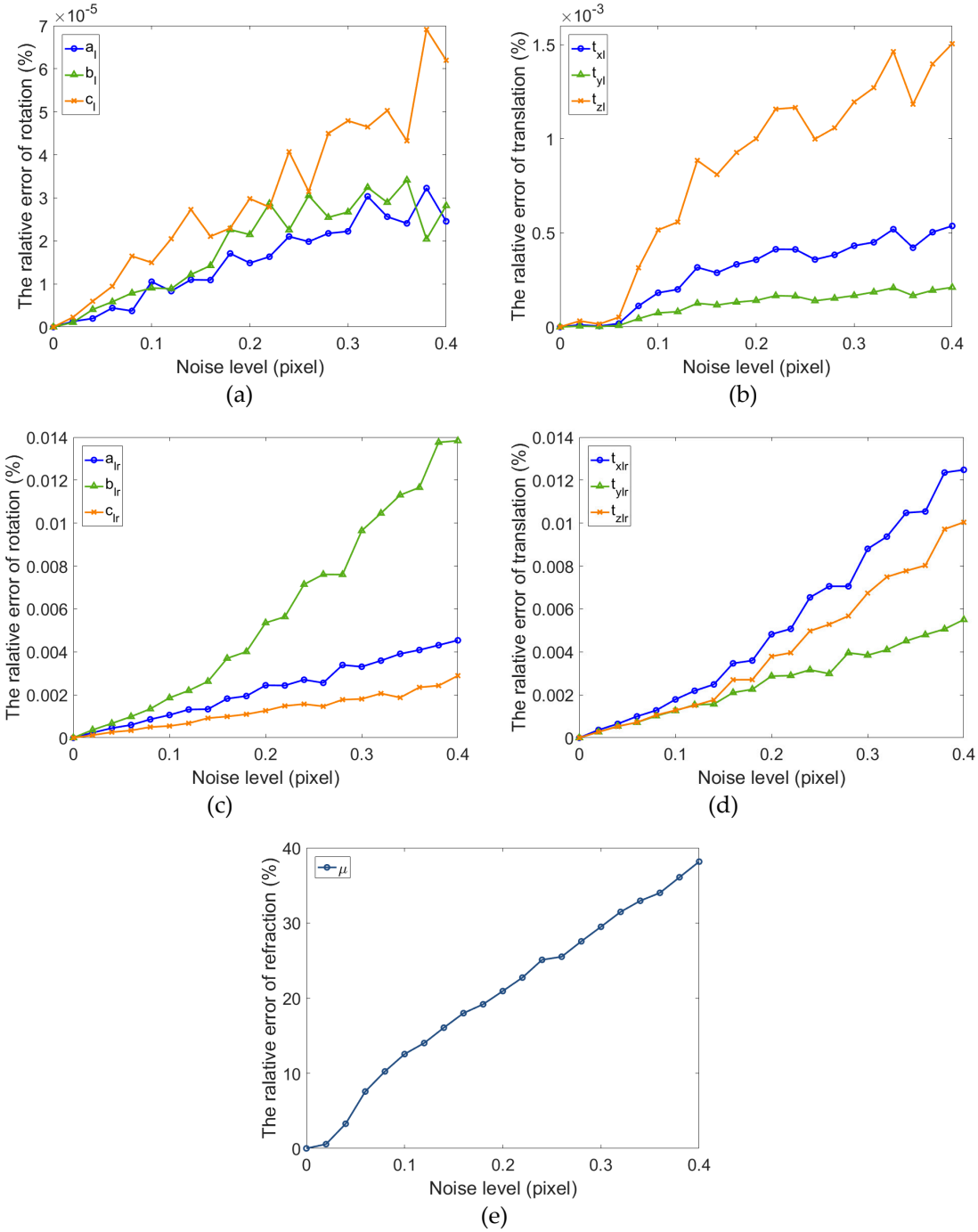

Figure 8. The relative error of extrinsic parameters for binocular camera with refraction estimation. (a) Relative error for rotation vector of left camera; (b) Relative error for translation vector of left camera; (c) Relative error for rotation vector of left and right camera; (b) Relative error for translation vector of left and right camera;(e) Relative error for refraction index.

In addition to the synthetic experiment of one camera, we have carried out a simulation experiment on multiple cameras using the refractive projection model (taking binocular camera as an example). This experiment is the same as a universal binocular camera because the left camera is a reference camera. The optimized parameters include the rotation and translation of the left camera relative to the world coordinate frame, and the rotation and translation of the right camera relative to the left camera. Meanwhile, the refractive index of glass is estimated and compared with single camera.

For binocular camera, Gaussian noise (mean = 0, std = 0-0.4) is also added to the images of left and right camera, respectively, then the calibration is conducted with these independent images for

Preprints (www.preprints.org) | NOT PEER-REVIEWED | Posted: 12 October 2017 doi:10.20944/preprints201710.0077.v1

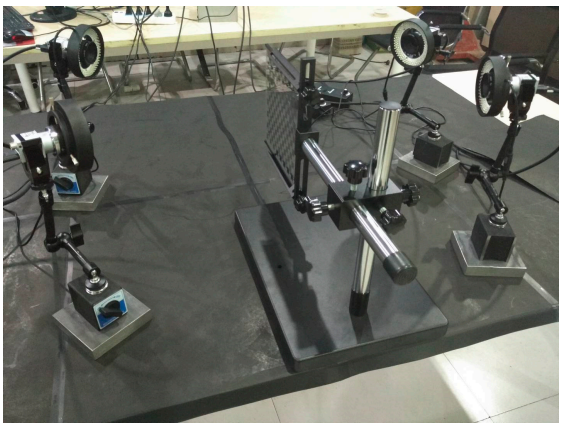

Figure 9. The 4-cameras system.

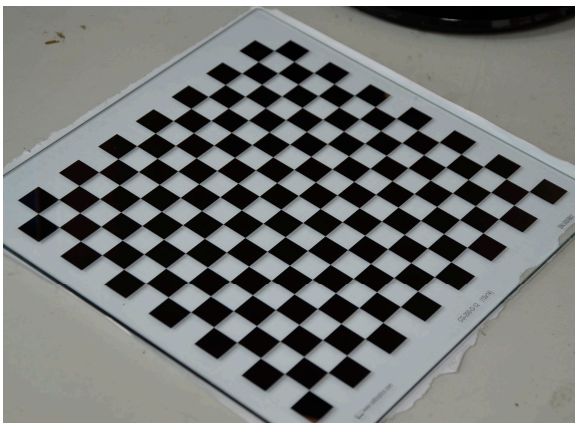

Figure 10. The glass calibration target.

100 times. Figure 8 shows the relative error of the extrinsic parameters of binocular camera and the refractive index. It can be seen from the figures that the rotation vector is more accurate than that of single camera. At the same time, the translation accuracy of binocular camera is lower than single camera. Due to the ray constraints of multiple direction of the binocular camera, the precision of estimated refractive index of binocular camera is significantly improved compared with single camera. Meanwhile, the accuracy of rotation and translation are relatively high.

4.2 Real Data

For the experiments with real data, all CMOS cameras (Basler acA2500-60uc) have the same configuration. The focal length of lens is 12.5mm and the image resolution of the camera is 2590x2048 pixels. The 4-cameras system is presented in Figure 9. As shown in Figure 10, the calibration target is a planar checkerboard with 14x13 corner points uniformly distributed. The size of the checkerboard is 200x200 mm^2 and the distance between the adjacent points is 12 mm in the horizontal and the vertical directions. The checkerboard pattern is printed on one side of glass calibration plate with position accuracy of 0.0015 mm.

Because it's possible to install one camera or multiple camera on one side of the measured object. Similar to the synthetic experiment, the experiments of real data will verify the calibration accuracy of one camera, binocular camera and 4-cameras system. Four cameras are used to perform these experiments using refractive projection model. Meanwhile, reflection and overlapping FOV of all cameras can lead to the restriction of positioning the calibration target and the inconvenience of operating the calibration target in the actual application. In order to improve the accuracy and convenience of the proposed method, the intrinsic parameters of all camera are calibrated first and then the extrinsic parameters are calibrated using the proposed calibration method. In the calibration process of intrinsic parameters, the cameras are fixed according to the size of the object and 21 images are taken from different orientations. Table 1 shows the intrinsic parameters of camera 1-4 obtained through Zhang's flexible calibration method [19]. As Table 1 illustrated, only the distortion coefficients k_1 and k_2 are listed.

The extrinsic parameters of one camera and multiple cameras, and refractive index of glass are solved by using the proposed method. We use the reprojection error of corner point to evaluate the accuracy of camera calibration. Figures 11-12 and 14 display the bivariate histogram of the unoptimized and optimized reprojection error of one camera, binocular cameras and four cameras. The reprojection errors of one camera (camera 4) are shown in Figures 11. It is obviously that the reprojection errors improve significantly through the nonlinear optimization. The mean value and the standard deviation of the initial reprojection errors are 0.0011 pixel and 0.1452 pixel, respectively. After the optimization, the mean value of the reprojection errors is -0.00003 pixel and the standard deviation is 0.0949 pixel. The calibration result of binocular camera (camera 3, 4) is shown in Figure 12. The comparison between the results of refractive calibration and the initial value shows that the bundle adjustment with refractive projection model is more reliable and more accurate. The mean value and standard deviation of reprojection errors change from 0.2842 and 0.6791 pixel to -0.0005

Preprints (www.preprints.org) | NOT PEER-REVIEWED | Posted: 12 October 2017 doi:10.20944/preprints201710.0077.v1

and 0.2213 pixel. The optimized extrinsic parameters of binocular camera are used to calculate the 3D position of the corner point. Then the position error is calculated based on the 3d position and the theoretical value. As shown in the Figure 13, the position error of optimized extrinsic parameters has been reduced to half of the unoptimized one.

In one camera and binocular camera system, we only use the refractive projection model. Four cameras are distributed on both sides of the glass calibration plate, which simultaneously uses the direct projection model and the refractive projection model. The 4-cameras system is used to verify the practicability of our presented method. Figure 14 shows the reprojection error of the 4-cameras system. The mean value and standard deviation of reprojection error change from -0.3378 and 2.9542 pixel to 0.00007 and 0.4543 pixel. We can discover that the standard deviation of reprojection errors is basically linear to the number of cameras. The optimized calibration results indicate that the stability and accuracy of our proposed method in real data experiments. The relative extrinsic parameters of 4-cameras system are reported in Table 2.

Table 1. The intrinsic parameters of four cameras.

	Camera 1	Camera 2	Camera 3	Camera 4
Focal Length	$\begin{bmatrix}2618.29\\2618.20\end{bmatrix}$	$\begin{bmatrix}2625.76\\2625.61\end{bmatrix}$	$\begin{bmatrix}2617.17\\2616.88\end{bmatrix}$	$\begin{bmatrix}2620.34\\2620.35\end{bmatrix}$
Principal point	$\begin{bmatrix}1290.91\\1014.72\end{bmatrix}$	$\begin{bmatrix}1286.45\\1001.44\end{bmatrix}$	$\begin{bmatrix}1255.36\\1026.86\end{bmatrix}$	$\begin{bmatrix}1293.70\\1006.56\end{bmatrix}$
Distortion $(k_1\ k_2)$	$\begin{bmatrix}-0.1338\\0.1326\end{bmatrix}$	$\begin{bmatrix}-0.1356\\0.1462\end{bmatrix}$	$\begin{bmatrix}-0.1332\\0.1360\end{bmatrix}$	$\begin{bmatrix}-0.1324\\0.1344\end{bmatrix}$

Table 2. The relative extrinsic parameters of 4-cameras system.

	Camera 2-1	Camera 3-1	Camera 4-1
Rotation Vector	$\begin{bmatrix}0.0892\\0.7389\\0.0365\end{bmatrix}$	$\begin{bmatrix}0.1479\\3.0076\\0.2330\end{bmatrix}$	$\begin{bmatrix}0.0212\\-2.3761\\-0.1040\end{bmatrix}$
Translation vector	$\begin{bmatrix}-248.9713\\1.0768\\93.0314\end{bmatrix}$	$\begin{bmatrix}-4.3414\\-81.7511\\766.3633\end{bmatrix}$	$\begin{bmatrix}274.9126\\-42.0589\\641.0544\end{bmatrix}$

4.3 Discussion

The above experiments based on synthetic and real data verify the accuracy and effectiveness of the proposed method. This method is applicable to the multi-cameras measurement system which can perform a one-shot measurement of the dynamic shape of whole part. The typical MCS is shown in Figure 5, and the cameras are distributed both sides of the glass calibration plate. Several patterns were designed for multi-cameras calibration, which can be grouped into three categories: 1D pattern, 3D target consisted of 1D patterns, and planar pattern. Compared with planar pattern, the disadvantage of other two calibration targets is that's hard to guarantee the exact linearity and the extraction accuracy of the points. However, the opaque planar pattern is difficult to complete multi-cameras calibration and it is easy to generate cumulative errors. With the help of the precision manufacturing technique, transparent glass calibration target can overcome the above limitations and complete the calibration of MCS. The position accuracy of corner point on commercial glass calibration plate can reach 0.0015 mm, so it can satisfy the precision requirement of multi-cameras calibration. The extrinsic parameters can be optimized in the global coordinates, and the refractive projection model is used to eliminate the refractive effect.

Preprints (www.preprints.org) | NOT PEER-REVIEWED | Posted: 12 October 2017 doi:10.20944/preprints201710.0077.v1

However, the proposed method also shows some limitations. Due to the reflection of glass, the camera's distribution and the calibration accuracy of multiple cameras are affected. In the calibration process of this paper, a few reprojection error can occur with abnormal value, which is caused by the reflection. Fortunately, the number of these outliers are very small and have little impact on the calibration results. Alternatively, we can delete these outliers and reduce the impact on the calibration results. It can also improve the reflection from the production process. In addition, the calibration method cannot be applied to the multi-cameras calibration without overlapping FOV.

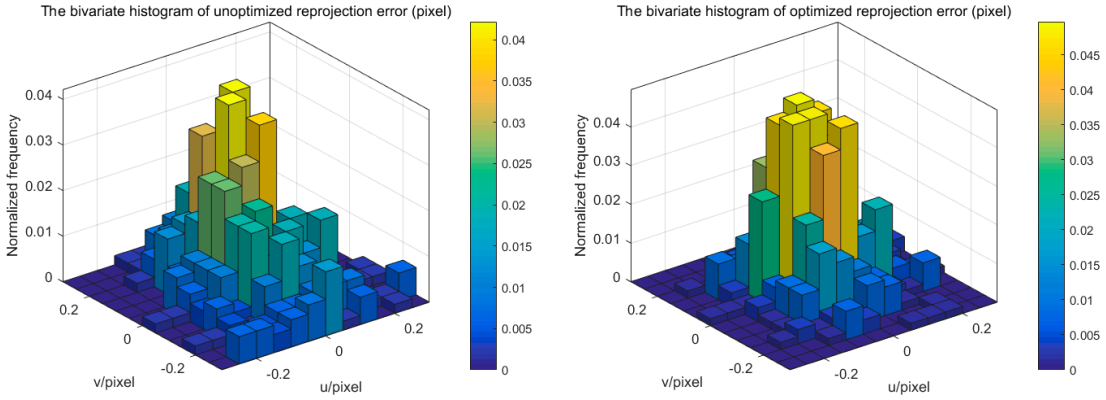

(a) (b)

Figure 11. The reprojection error of one camera. (a) unoptimized (b) optimized

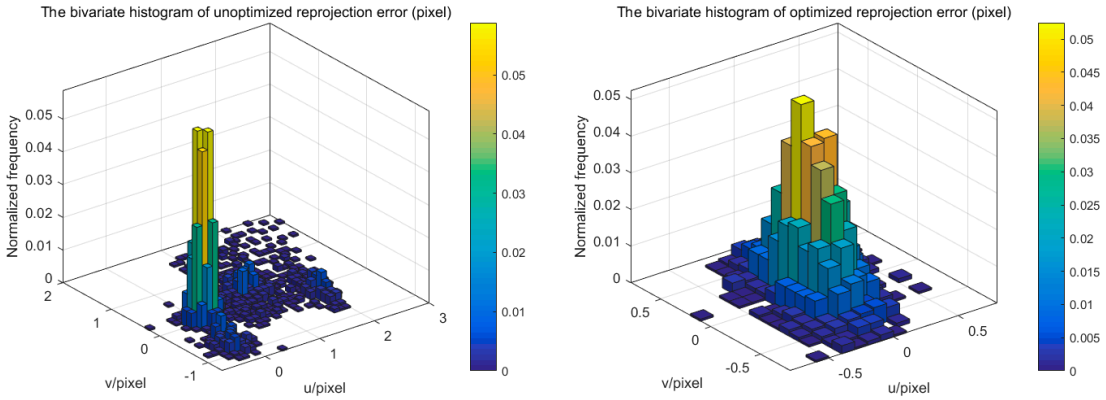

(a) (b)

Figure 12. The reprojection error of binocular camera. (a) unoptimized (b) optimized

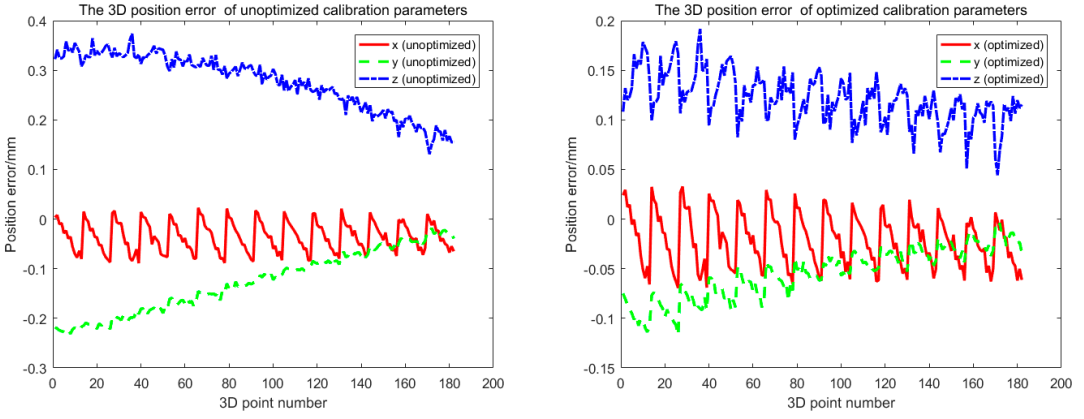

(a) (b)

Figure 13. The 3D position error using binocular camera. (a) unoptimized (b) optimized

Preprints (www.preprints.org) | NOT PEER-REVIEWED | Posted: 12 October 2017 doi:10.20944/preprints201710.0077.v1

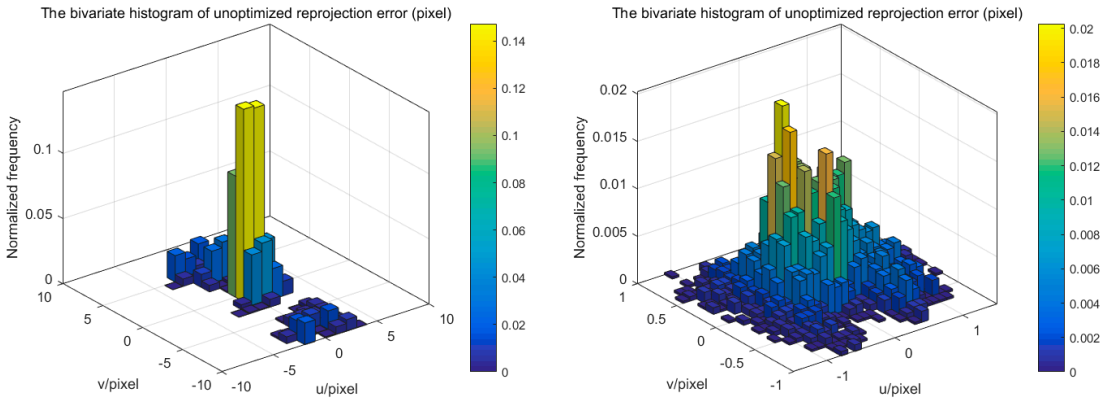

(a) (b)

Figure 14. The reprojection error of one camera. (a) unoptimized (b) optimized

5. Conclusions

One typical MCS is installed on both sides of the measured object, which makes it difficult to calibrate the system using the existing camera calibration methods. In this paper, a novel multi-cameras calibration method based on glass calibration plate and ray tracing is proposed. Based on the traditional direct projection model, the refractive projection model is developed and the model is applied for multi-cameras calibration. Firstly, the mathematical models of refractive projection and bundle adjustment are established with introduction of ray tracing. Then, the intrinsic parameters of each camera is obtained by Zhang's calibration method and direct linear transformation is used to obtain the initial extrinsic parameters. Finally, the modified bundle adjustment method is applied to optimize the extrinsic parameters of MCS and the refractive index of glass calibration target. The experimental results of refractive calibration show that the error of the 3D reconstruction is smaller than 0.2 mm, the relative errors of both rotation and translation are less than 0.014%, and the mean and standard deviation of reprojection error of 4-cameras system are 0.00007 and 0.4543 pixel. The experiments performed on synthetic and real data indicate that our proposed method has high-accuracy and feasibility.

Acknowledgments: This work has been supported by National Natural Science Foundation of China (Grant No. 51505054, 51705057), Chongqing Science and Technology Commission (Grant No. cstc2015zdcy-ztzx60002, cstc2016jcyjA1613, cstc2015zdcy-ztzx30001, cstc2014jcyjA60003), Scientific and Technological Research Program of Chongqing Municipal Education Commission (Grant No. KJ1500405, CYS17233).

Author Contributions: The paper was a collaborative effort between the authors. Mingchi Feng and Xiang Jia proposed the idea of the paper. Mingchi Feng, Xiang Jia, and Song Feng implemented the algorithm, designed and performed the experiments. Mingchi Feng, Jingshu Wang, and Taixiong Zheng analyzed the experimental results and prepared the manuscript.

Conflicts of Interest: The authors declare no conflict of interest.

References

1. Zhan, D.; Yu, L.; Xiao, J.; Chen, T.L. Multi-camera and structured-light vision system (msvs) for dynamic high-accuracy 3d measurements of railway tunnels. *Sensors-Basel* **2015**, *15*, 8664-8684. 10.3390/s150408664
2. Gong, Z.; Liu, Z.; Zhang, G.J. Flexible global calibration of multiple cameras with nonoverlapping fields of view using circular targets. *Appl Optics* **2017**, *56*, 3122-3131. 10.1364/Ao.56.003122
3. Bosch, J.; Gracias, N.; Ridao, P.; Ribas, D. Omnidirectional underwater camera design and calibration. *Sensors-Basel* **2015**, *15*, 6033-6065. 10.3390/s150306033
4. Schmidt, A.; Kasiński, A.; Kraft, M.; Fularz, M.; Domagała, Z. Calibration of the multi-camera registration system for visual navigation benchmarking. *Int J Adv Robot Syst* **2014**, *11*, 83. 10.5772/58471

5. Ryan, D.; Denman, S.; Fookes, C.; Sridharan, S. Scene invariant multi camera crowd counting. *Pattern Recogn Lett* **2014**, *44*, 98-112. 10.1016/j.patrec.2013.10.002
6. Kovac, I. In *Flexible inspection systems in the body-in-white manufacturing*, Proceedings of the 2004 International Workshop on Robot Sensing, May 24, 2004 - May 25, 2004, Graz, Austria, 2004; Institute of Electrical and Electronics Engineers Inc.: Graz, Austria, pp 41-48. 10.1109/ROSE.2004.1317612
7. Chen, X.; Yang, L.X.; Xu, N.; Xie, X.; Sia, B.; Xu, R. Cluster approach based multi-camera digital image correlation: Methodology and its application in large area high temperature measurement. *Opt Laser Technol* **2014**, *57*, 318-326. 10.1016/j.optlastec.2013.08.005
8. Chen, F.X.; Chen, X.; Xie, X.; Feng, X.; Yang, L.X. Full-field 3d measurement using multi-camera digital image correlation system. *Opt Laser Eng* **2013**, *51*, 1044-1052. 10.1016/j.optlaseng.2013.03.001
9. Weng, J.; Cohen, P.; Herniou, M. Camera calibration with distortion models and accuracy evaluation. *IEEE Transactions on Pattern Analysis and Machine Intelligence* **1992**, *14*, 965-980. 10.1109/34.159901
10. Shen, E.; Hornsey, R. Multi-camera network calibration with a non-planar target. *Ieee Sens J* **2011**, *11*. 10.1109/Jsen.2011.2123884
11. Zhang, Z. A flexible new technique for camera calibration. *IEEE Transactions on Pattern Analysis and Machine Intelligence* **2000**, *22*, 1330-1334. 10.1109/34.888718
12. Dong, S.; Shao, X.X.; Kang, X.; Yang, F.J.; He, X.Y. Extrinsic calibration of a non-overlapping camera network based on close-range photogrammetry. *Appl Optics* **2016**, *55*, 6363-6370. 10.1364/Ao.55.006363
13. Baker, P.T.; Aloimonos, Y. In *Calibration of a multicamera network*, 2003 Conference on Computer Vision and Pattern Recognition Workshop, 16-22 June 2003, 2003; pp 72-72. 10.1109/CVPRW.2003.10085
14. Belden, J. Calibration of multi-camera systems with refractive interfaces. *Exp Fluids* **2013**, *54*, 1463. 10.1007/s00348-013-1463-0
15. Orteu, J.J.; Bugarin, F.; Harvent, J.; Robert, L.; Velay, V. Multiple-camera instrumentation of a single point incremental forming process pilot for shape and 3d displacement measurements: Methodology and results. *Exp Mech* **2011**, *51*, 625-639. 10.1007/s11340-010-9436-1
16. Zhengyou, Z. Camera calibration with one-dimensional objects. *IEEE Transactions on Pattern Analysis and Machine Intelligence* **2004**, *26*, 892-899. 10.1109/TPAMI.2004.21
17. Wang, L.; Wang, W.W.; Shen, C.; Duan, F.Q. A convex relaxation optimization algorithm for multi-camera calibration with 1d objects. *Neurocomputing* **2016**, *215*, 82-89. 10.1016/j.neucom.2015.07.158
18. Liu, Z.; Li, F.J.; Zhang, G.J. An external parameter calibration method for multiple cameras based on laser rangefinder. *Measurement* **2014**, *47*, 954-962. 10.1016/measurement.2013.10.029
19. Fu, Q.; Quan, Q.; Cai, K.Y. Calibration of multiple fish-eye cameras using a wand. *Iet Comput Vis* **2015**, *9*, 378-389. 10.1049/iet-cvi.2014.0181
20. Loaiza, M.E.; Raposo, A.B.; Gattass, M. Multi-camera calibration based on an invariant pattern. *Comput Graph-Uk* **2011**, *35*, 198-207. 10.1016/j.cag.2010.12.007
21. de Franca, J.A.; Stemmer, M.R.; Franca, M.B.D.; Piai, J.C. A new robust algorithmic for multi-camera calibration with a 1d object under general motions without prior knowledge of any camera intrinsic parameter. *Pattern Recogn* **2012**, *45*, 3636-3647. 10.1016/j.patcog.2012.04.006
22. Shin, K.Y.; Mun, J.H. A multi-camera calibration method using a 3-axis frame and wand. *Int J Precis Eng Man* **2012**, *13*, 283-289. 10.1007/s12541-012-0035-1
23. Long, Q.; Zhongdan, L. Linear n-point camera pose determination. *IEEE Transactions on Pattern Analysis and Machine Intelligence* **1999**, *21*, 774-780. 10.1109/34.784291
24. Xu, G.; Zhang, X.; Li, X.; Su, J.; Hao, Z. Global calibration method of a camera using the constraint of line features and 3d world points. In *Measurement Science Review*, 2016; Vol. 16, p 190. 10.1515/msr-2016-0023

25. Tsai, M.-J.; Hung, C.-C. Development of a high-precision surface metrology system using structured light projection. *Measurement* **2005**, *38*, 236-247. 10.1016/j.measurement.2005.07.014
26. Tsai, R. A versatile camera calibration technique for high-accuracy 3d machine vision metrology using off-the-shelf tv cameras and lenses. *IEEE Journal on Robotics and Automation* **1987**, *3*, 323-344. 10.1109/JRA.1987.1087109
27. Huang, J.H.; Wang, Z.; Gao, Z.H.; Gao, J.M. A novel color coding method for structured light 3d measurement. *Proc Spie* **2011**, *8085*. 10.1117/12.889317
28. Mulsow, C. A flexible multi-media bundle approach. *Int. Arch. Photogramm. Remote Sens. Spatial Inf. Sci* **2010**, 472-477.
29. Hartley, R.I. In defense of the eight-point algorithm. *IEEE Transactions on Pattern Analysis and Machine Intelligence* **1997**, *19*, 580-593. 10.1109/34.601246
30. Agrawal, A.; Ramalingam, S.; Taguchi, Y.; Chari, V. In *A theory of multi-layer flat refractive geometry*, 2012 IEEE Conference on Computer Vision and Pattern Recognition, 16-21 June 2012, 2012; pp 3346-3353. 10.1109/CVPR.2012.6248073